Inhibiting the Carbon Deposition from the Reverse Boudouard Reaction in Refractories Submitted to CO–H_2 Atmosphere

J. Poirier, J. Kadok, N. Bost, A. Coulon, M. R. Ammar, S. Brassamin, C. Genevois

The catalytic decomposition of carbon monoxide via the reverse Boudouard reaction in the presence of a mixture of CO–H_2 gas produces a solid sp^2 carbon deposit, which has deleterious effects on refractory materials.

The catalytic effects of iron oxides and the structural evolution of carbon during the reverse Boudouard reaction in CO–H_2 atmosphere is investigated at a nano and micro-scale. Sulphur compounds inhibit the carbon monoxide dissociation on contact with iron and iron oxides. The samples were characterised by X-ray diffraction, Raman spectroscopy, scanning and transmission electron microscopy. A mechanism that governs the inhibition of the reaction is proposed and validated at lab scale, in which the formation of a very thin protective FeS layer (0,5–1 nm) is involved. This research is applied to develop ew CO/H_2 resistant refractories.

1 Introduction

The mechanism of carbon monoxide decomposition, called the reversed Boudouard reaction:

$2CO_{(g)} \rightarrow CO_{2(g)} + C_{(s)}$ results in the deposition of sp^2 solid carbon. This C deposition, inside the porosity of the refractory, causes premature degradation of linings, which operate under reducing atmosphere [1]. The destruction of refractory materials in CO atmosphere is well explained in the literature [2].

The refractory damage process includes four steps:

- diffusion of CO gas diffusion into the porosity of the refractory material;
- reduction of iron oxides into iron then carburation into Fe_3C, which then acts as a catalyst for C-decomposition according $Fe_3C \rightarrow 3\ Fe + C$;
- nucleation and growth of the carbon deposition, which generate thermomechanical stress inside the refractory;
- formation of cracks, damage then destruction of the refractory.

This reaction occurs at temperature ranging between 400–900 °C with a maximum intensity around 600 °C and is highly favoured by the presence of catalytic particles such as iron and iron oxides. Fe_xO_y and Fe particles are present in the refractories as secondary mineral phases in raw materials and as impurities due to crushing and mixing while blending the refractory formulation.

The CO resistance is usually improved by the selection of raw materials with a low content of iron particles and by increasing the refractory sintering temperature (Fe ions are adsorbed in the lattice or bonded in the glassy phase). However, these solutions are not always very effective for industrial applications (such as low-CO blast furnace process, biomass gasification reactors, steam methane reformers, direct reduction shafts, reactors in the petrochemical industry, etc.) where refractories are subjected to CO and H_2 extremely reducing atmospheres.

According to the literature, two reactions explain the carbon deposition phenomena in a temperature range between 400–1050 °C:

- the reverse Boudouard reaction

$$2\ CO = C + CO_2$$
$$\Delta H° = -172{,}4\ \text{kJ/mol}$$
$$K_1 = P_{CO2} \cdot a_C / P_{CO2} \qquad (1)$$

- the reverse water gas reaction

$$CO + H_2 = C + H_2O$$
$$\Delta H° = -131{,}3\ \text{kJ/mol}$$
$$K_2 = P_{H2O} \cdot a_C / P_{CO} \cdot PH_2 \qquad (2)$$

From reactions (1) and (2), the water-gas shift reaction (WGSR) describes the reaction of carbon monoxide and water vapour to form carbon dioxide and hydrogen

$$CO + H_2O = CO_2 + H_2$$
$$\Delta H° = -41{,}166\ \text{kJ/mol}$$
$$K_3 = P_{CO2} \cdot P_{H2} / P_{CO} \cdot P_{H2O} \qquad (3)$$

In direct reduction processes, the decomposition of methane into carbon also occurs

$$CH_4 = C + 2\ H_2$$
$$\Delta H° = 92{,}676\ \text{kJ/mol}.$$
$$K_4 = P_{H2}^{\ 2} \cdot a_C / P_{CH4} \qquad (4)$$

J. Poirier, J. Kadok, N. Bost, A. Coulon, M. R. Ammar, S. Brassamin, C. Genevois
CNRS, CEMHTI UPR 3079
University of Orléans
Orléans, France

Corresponding author: *J. Poirier*
E-mail: jacques.poirier@univ-orleans.fr

Keywords: Boudouard reaction, carbon deposition, refractory damage, cementite, sulphur

The paper was awarded with the 1st Prize for Posters at ICR 2018

Fig. 1 Carbon deposition on a Fe_2O_3 sample after exposure to a gas mixture consisting of 71,0 % CO, 3,0 % CO_2, 11,0 % H_2 and 15,0 % N_2, for 5 h, at 600 °C

In reactions (1–4), K_1, K_2, K_3, K_4 are the equilibrium constants of reactions, P_{CO}, P_{CO2}, P_{H2}, P_{H2O}, P_{CH4} the partial pressures of CO, CO_2, H_2, H_2O, CH_4 and a_C the carbon activity. The effect of H_2 in CO increases significantly the reaction of carbon deposition. For example, Walker, et al. [3], report a deposition of 10 g of solid carbon after ≈350 min over 0,10 g of carbonyl iron in 9 %-H_2–91 % CO gas mixture at 602 °C.

Fig. 1 illustrates this reaction. Few grams of Fe_2O_3 were submitted to 71 % CO, 3 % CO_2, 11 % H_2, 15 % N_2 gas mixture during 5 h at 600 °C under atmospheric pressure. A large amount of carbon formation was observed similar to a "popcorn" formation. However, this phenomenon is not described in CO + H_2 atmosphere and the mechanism is not really understood.

The hydrogen content in the CO has an effect on the temperature at which the maximum rate of C-deposition occurs from ~530 °C for 0,8 % H_2 to 630 °C for 19,9 % H_2. Increasing the hydrogen content increases the amount of carbon formed.

This paper reports studies of the carbon formation by the Boudouard reaction using Fe_xO_y catalysts, and a CO + H_2 atmosphere, at 600 °C. The reaction of the carbon formation was investigated, in these extreme conditions, using thermogravimetric measurements and in situ Raman spectroscopy. After cooling, the samples were characterised using various methods: X-Ray Diffraction (XRD) and Scanning and Transmission Electron Microscopy (SEM and TEM).

The aims of this research are:

- to understand the effect of iron oxides on the carbon formation and to characterise the structural organisation of carbon obtained by the reverse Boudouard reaction in CO and H_2 atmosphere;
- to investigate the inhibition of the sp^2 carbon formation in refractories from CO disproportionation catalysed by iron oxides under the most favourable conditions of the reaction, i.e., in the presence of H_2 at 600 °C;
- to describe in detail the mechanisms of carbon inhibition. The effect of sulphur on the Boudouard reaction, catalysed by iron oxides in presence of H_2 gas, was investigated under laboratory conditions;
- to find an efficient solution to inhibit the carbon deposit and to limit the industrial degradations of refractories.

2 Materials and methods

Various iron oxide particles were used as the catalyst of the Boudouard reaction. The reducing gas mixture (71 % CO, 3 % CO_2, 11 % H_2, 15 % N_2), referred to as CO/H_2 gas, was similar to the gas mixture used in low-CO blast furnace industrial processes. Solid sulphur and sulphur dioxide are used as inhibitors of the Boudouard reaction (Tab. 1).

Laboratory experiments were also carried out with Fe_2O_3 powders mixed with solid sulphur and with $SO_{2(g)}$. $SO_{2(g)}$ was mixed continuously with the reducing CO/H_2 gas.

Measurements of Fe_2O_3 mass variation were performed using a thermobalance from NETZSCH STA 409C/CD coupled with a QMS 403/5 Skimmer. Fe_2O_3 samples of approximately 30 mg were placed in an alumina crucible and were heated to 600 °C at a rate of 10 C · min^{-1} under 100 ml · min^{-1} of an argon inert gas prior to being exposed to a reducing CO/H_2 gas (100 ml · min^{-1}).

The crystalline phases were analysed with powder X-ray diffraction using a Bruker D8 A25 diffractometer (Bragg-Brentano geometry θ-θ) equipped with a LynxEye XE detector and using the Cu K_α radiation (λ = 1,5418 Å). Raman spectroscopy was performed using a T64000 Jobin-Yvon multichannel spectrometer equipped with an Ar–Kr laser source, aBX41 Olympus microscope and a liquid nitrogen-cooled CCD detector.

The spectra were collected in a backscattering geometry under a microscope (×20 long working distance objective) using the 514,5 nm wavelength (2,41 eV; 3 mW of laser power), a 600 groves · mm^{-1} grating giving a spectral resolution of 3 cm^{-1} in the 1000–2000 cm^{-1} wavenumber range. Heating the sample was achieved using a TS1500 Linkam device (Tadworth/GB).

The same temperature program was used for Raman spectroscopy and for TGA (10 °C · min^{-1} until 600 °C). After the experiments, the samples were also characterised by scanning electron microscopy (Hitachi S4500 FEG) and high resolution transmission electron microscopy (Philips CM20 microscope).

Scanning transmission electron microscopy high angle annular dark field (STEM-HAADF) images were acquired in the angular range of 50–180 mrad with an 8 cm camera length and a 0,1 nm probe size. Elemental composition line scans were performed by STEM-EDS using a JEOL EDS system and a 0,13 nm probe size.

Tab. 1 Origin and purity of the raw materials

	Materials	Origin	Purity [mass-%])	Particle Size [µm]	Specific Surface Area [m²/g]
Catalysts	Fe	Sigma Aldrich	>99	2–5	2
	FeO	Sigma Aldrich	99,9	2–5	6
	Fe_3O_4	LKAB	>99	2–5	2
	Fe_2O_3	Sigma Aldrich	>99	2–5 [a]	8.0
		Sigma Aldrich	>99	0,0035 [a]	42
		Carajas	>98	160–250	10,5
		Carajas	>98	1000–2000	3,7
Reducing gas	CO/H_2	Air Liquide	>99.9		
Sulphur dioxide	$SO_{2\ (g)}$	Air Liquide	>99,9		
Solid sulphur	S	Alfa Aesar	>99,5	≤10 [b]	

[a] Data as provided by the Sigma-Aldrich Company, [b] Prepared by grinding in an agate mortar

3 Effect of iron oxides on the carbon formation in CO, H_2 atmosphere [2]

3.1 Effect of Fe_2O_3 grain size on the rate of carbon formation

Fe_2O_3 with different grain sizes (35 nm, <5 µm, 160–250 µm and 1–2 mm/purity >99 %) was used. Initial specific surfaces of the particles are below 10 m^2/g, excepted for the 35 nm size (42 m^2/g). Fig. 2 a shows the variation in the sample weight (full lines) based on the thermogravimetric measurements (TGA) as well as the variation in the temperature (black dashed line) as a function of time. At 600 °C, the samples were subjected to a CO/H_2 gas mixture (composition R: 71 % CO, 3 % CO_2, 11 % H_2, 15 % N_2) for 5 h.

As soon as the gas was injected (at approximately 130 min), a weight loss (approximately 25 mass-% for the nanometre grain size) that was associated with the reduction of the Fe_2O_3 phase in competition with the production of solid carbon was observed. After this reduction, a rapid increase in the weight of the samples was observed (Fig. 2 a). This weight gain was primarily due to the production of solid carbon and corresponded to a catalyst/carbon deposition ratio of approximately 1/100 within the asymptotic limit of the Fe_2O_3 sample. Fig. 2 b shows the normalised weight curve using an asymptotic function of the curves shown in Fig. 2 a. According to the data, the production of carbon appears to be independent of the grain size of the catalyst; the size of the initial grain is not an important parameter for controlling the rate of carbon deposition. However, the smallest grains (35 nm) were slightly more reactive and formed more carbon than the largest grains. The largest grains exhibited the slowest formation and produced less carbon.

3.2 Effect of the iron valence on the carbon deposition rate

Pure iron and iron oxides (FeO, Fe_2O_3 and Fe_3O_4) powders were submitted for 5 h at 600 °C under reducing atmosphere (composition R 70 % CO, 10 % H_2, 3 % CO_2 and 17 % N_2).

The gas flow was 4,2 l/h. Results are reported in Fig. 3 a. As soon as the gas was injected (at ≈130 min), a weight loss (≈25 % for Fe_2O_3; Fig. 3 b) that was associated with the chemical reduction of the Fe_xO_y phase occurs. After this reduction, a rapid increase in the weight of all of the samples was observed, except for the FeO sample, which requires a longer reaction time (≈50 min). The reaction produces a large amount of solid carbon (Fig. 3 c).

The Fe_xO_y particles are reduced to metallic iron by the hydrogen. This phenomenon has been described in the literature [3, 4]. In a mixture consisting of CO+H_2 gas, there are many competing reactions including chemical reduction of iron oxides, carbon deposit via the reverse Boudouard reaction, and water and carbon formation via the reverse water-gas reactions. It is impossible to distinguish these different reactions in thermogravimetric measurements.

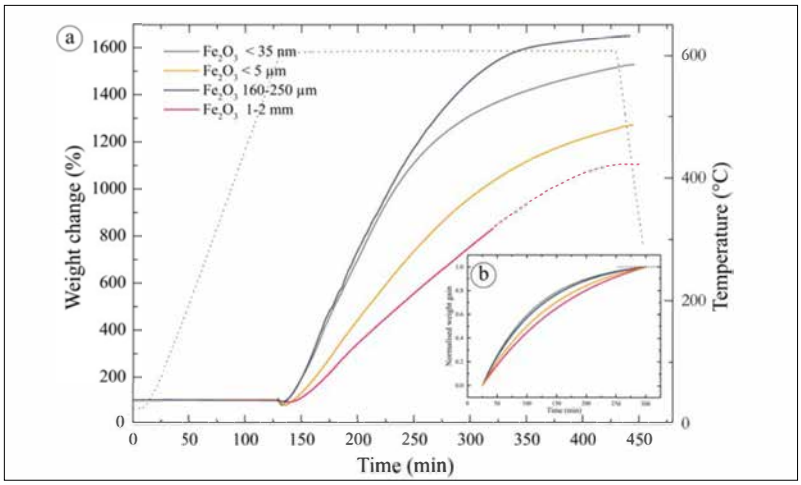

Fig. 2 a–b a) Mass variation of Fe_2O_3 samples versus time depending to the temperature (in black dotted line); b) mass normalised curve

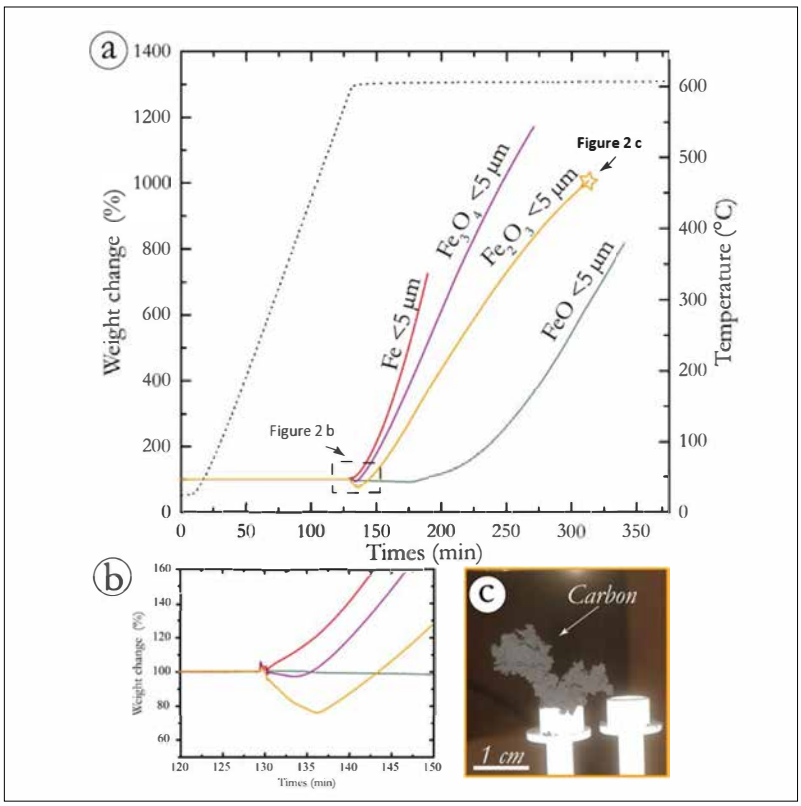

Fig. 3 a–c a) Mass variation of the sample as a function of time and temperature (in dotted line); b) enlargement of the Fig. 3 a; c) carbon deposition in the crucible for the Fe_2O_3 samples

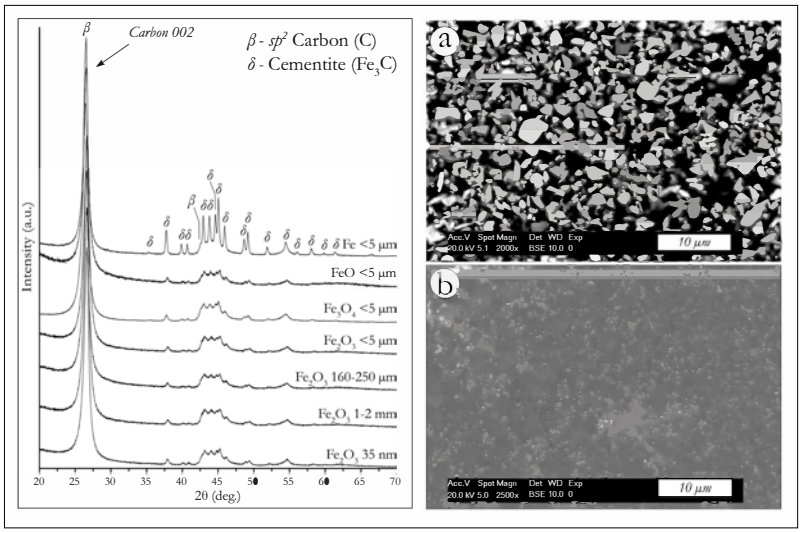

Fig. 4 a–b a) XRD diffractograms of the Fe_xO_y samples and backscattered images initial sample Fe_2O_3 <5 µm; b) after the CO–H_2 reaction, the size of particles is reduced

Complementary measurements: XRD and SEM observations (Fig. 4) show the quasi complete transformation of a few milligrams of Fe_xO_y in pure cementite phase (Fe_3C). The sp^2 type carbon is formed and is favoured by the catalyst particles. The catalyst grains are highly fragmented to nanometre-sized grains independently of the initial grain size, due to hydrogen effect and the chemical reduction. During the experiment, the Fe_xO_y particles were substantially reduced in size.

4 Effect of sulphur compounds on the inhibition of the carbon formation

This part presents an efficient method to inhibit the carbon deposit from the reverse Boudouard reaction catalysed by the Fe_xO_y oxides: a low quantity of sulphur additions prevents the formation of carbon [5]. TGA experiments were performed to quantify the effect of inhibiting sulphur on carbon growth rate as a function of the S amount in the various solid or gaseous mixtures.

4.1 Effect of solid sulphur on the amount of carbon produced by the Boudouard reaction

TGA experiments were performed to validate the effect of inhibiting sulphur compounds on carbon formation, and to quantify the carbon growth rate in function of the S amount and sulphur species in the various mixtures. Fe_2O_3 powders were mixed with sulphur with different amount (1, 5, 10 and 30 mass-% S respectively) and with sulphates (1 mass-% $BaSO_4$, 1 mass-% $CaSO_4$, 1 mass-% $MgSO_4$). Fig. 5 a–b shows TGA results (mass variation as a function in time) and are compared to an experiment without sulphur or sulphates additions.

During heating, in inert atmosphere (100 ml · min^{-1} Ar), Fe_2O_3 + S mixtures have a mass loss associated with sulphur vaporization at 443 °C, proportional to the amount of the introduced S (Fig. 5 a). This loss of mass is not observed for the mixtures: Fe_2O_3 – 1 mass-% $BaSO_4$, $CaSO_4$, $MgSO_4$ (Fig. 5 b). Indeed, the decomposition of sulphates and thus the volatilization of S occur at temperatures above 600 °C. As soon as the CO/H_2 reducing gas is injected, a weight loss (approximately 25 mass-%) is observed which is due to the chemical reduction of the iron oxides by hydrogen. The Fe_2O_3 sample (reference) shows a very important carbon deposit. The samples containing sulphur and sulphates have a very low weight gain that stabilizes after 200 min.

4.2 Effect of S gas on the amount of carbon produced by the Boudouard reaction

The continuous injection of gaseous sulphur has many advantages compared to a solid sulphur addition. It allows providing a sustainable amount of sulphur and thus, a more efficient inhibition of carbon formation. The experiments were carried out with

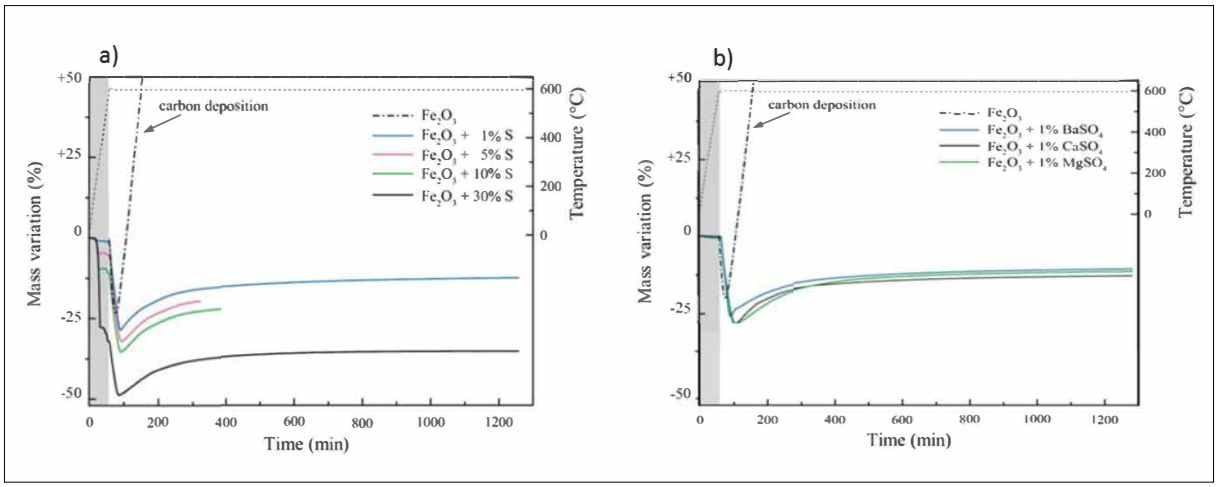

Fig. 5 a–b TGA curves of the samples exposed to the reducing gas mixture at 600 °C:
a) mixture of Fe_2O_3 powders and pure S (1, 5, 10 and 30 mass-%, respectively);
b) mixture of Fe_2O_3 powders and sulphates (1 mass-% $BaSO_4$, 1 mass-% $CaSO_4$ and 1 mass-% $MgSO_4$)

Fe_2O_3 at 600 °C under a CO/H_2 reducing gas containing $SO_{2(g)}$.

Fig. 6 shows TGA results (mass variation as a function of time) for $SO_{2(g)}$ contents equal to 1, 10, 50, 100 and 1000 ppm, respectively and compared to an experiment without $SO_{2(g)}$ addition. Once the gas mixture is injected, all samples underwent a similar mass loss for about 20 min. This is the consequence of the Fe_2O_3 reduction into pure iron prior to its carburation in iron carbide [6]. For the samples exposed to a gas mixture containing 1–10 ppm of $SO_{2(g)}$, a dramatic mass gain is observed due to carbon formation; roughly like what could be found without $SO_{2(g)}$. When 50 ppm of SO_2 was injected, a lower mass gain is observed, and the carbon growth rate has been decreased by a factor 5 in comparison with the experiment without SO_2. For 100 ppm and 1000 ppm of SO_2, the carbon growth rate values have been decreased by a factor 70. However, a slightly higher mass gain is observed for the sample with 100 ppm of SO_2 in comparison with 1000 ppm.

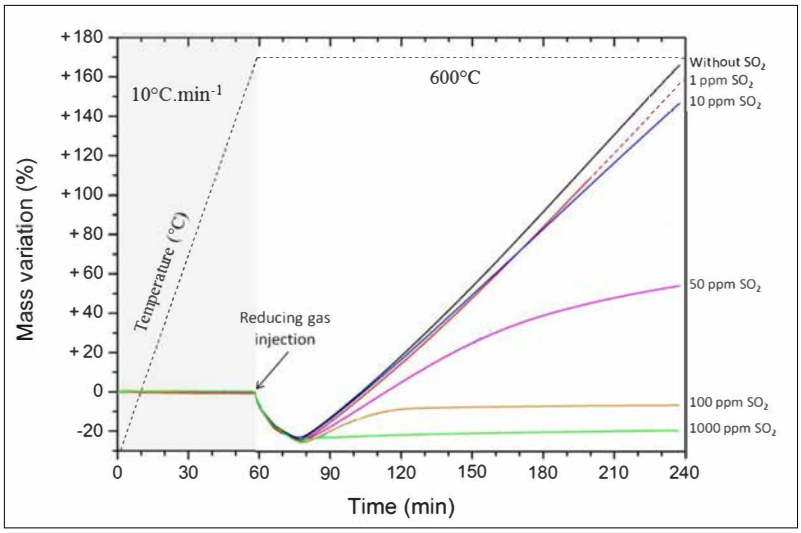

Fig. 6 TGA curves of the Fe_2O_3 samples exposed to the reducing gas mixture containing small fractions of SO_2 at 600 °C (continuous curves)

4.3 Structural evolution of the carbon

4.3.1 Raman spectroscopy

Raman spectroscopy is an ideal technique to characterize in situ sp^2 carbon materials. It is the most sensitive to explore the full range of the structural states from perfectly crystalline to amorphous [7].

The typical Raman spectrum of sp^2 carbon is reported in Fig. 7 c and shows three prominent features. The so-called G band located at approximately 1580 cm^{-1} corresponds to the in-plane bond stretching of carbon atoms (E_{2g} symmetry). When defects are present, the crystal symmetry breaks down and additional bands appear at specific frequencies depending on the excitation energy used. These bands are called the defect bands: D (≈1250–1400 cm^{-1}) and D' (≈1600–1630 cm^{-1}). At relatively low defect density, the intensity ratio of the defect-induced D band and the symmetry-allowed G band increases with disorder.

Pure iron and iron oxides powders were submitted for 30 min at 600 °C under reducing atmosphere: 100 % CO and CO/H_2 mixture.

Fig. 7 summarizes the results obtained using Raman spectroscopy and TEM. Raman spectra of the carbon formed in the two types of gas are totally different. G band is observed in the carbon formed under 100 % CO, and D and G bands are observed when the gas is a mixture of CO and H_2.

In CO atmosphere, well organised sp^2 carbon is formed around the catalyst particles and the defect-induced D bands are not observed. Only chemical reduction of the catalyst particle occurs without significant size reduction. Therefore, poly-aromatic layers are formed around the catalyst particles in the form of encapsulating shells. These layers are sufficiently large with regards to the laser diameter which explains the no activation of the defect-induced D band in the corresponding Raman spectrum [6]. In $CO + H_2$ atmosphere, the corresponding Raman spectrum exhibits the defect induced D band suggesting disordered carbon. Catalyst particles are chemically reduced and

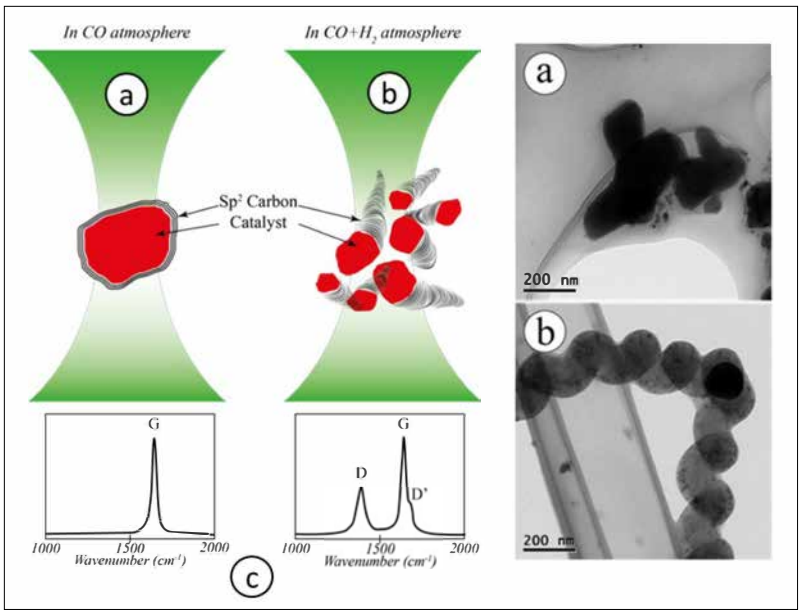

Fig. 7 a–c Schematic representation of the interaction of the Raman excitation laser and the carbon particles in shell around catalyst particles in 100 % CO and in nano-fibres in $CO + H_2$ atmosphere. TEM micrographs of nano-carbon shells and filaments formed à 600 °C in: a) 100 % CO; and b) 70,0 % CO, 3,0 % CO_2, 10,0 % H_2 and 17,0 % N_2 from Fe_2O_3 nanometer size catalyst

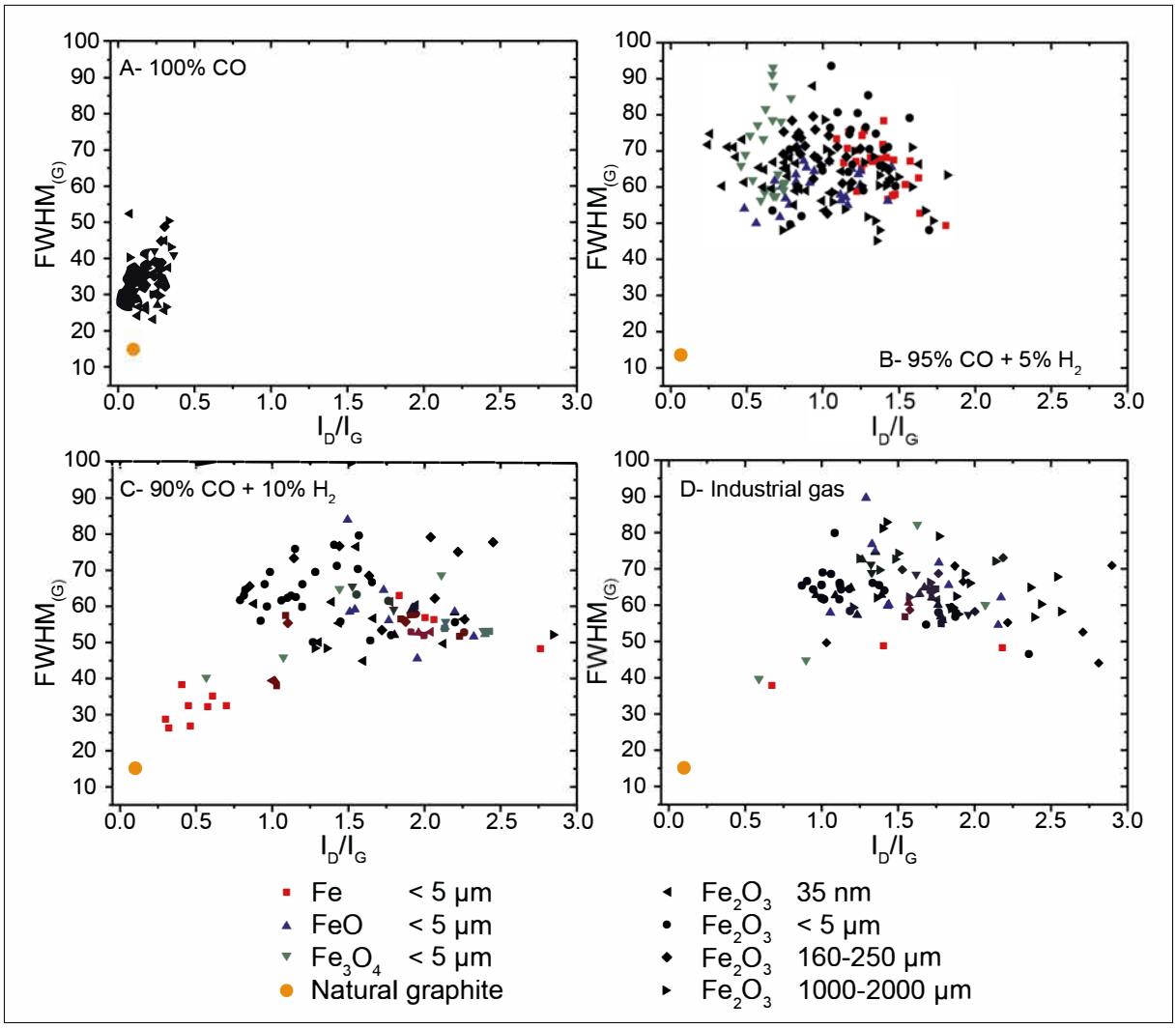

Fig. 8 Evolution of G band width at half-maximum ($FWHM_{(G)}$) versus the intensity ration of the D relative to G band of series of in situ measurement of carbon formed under different iron catalyst at different gases at 600 °C (except for C at 500 °C)

highly fragmented. Therefore, small-sized carbon nanofibres are formed exhibiting a large amount of poly-aromatic boundaries. This eventually leads to the activation of the defect induced D band without the local structural order being necessarily disturbed [6].

Fig. 8 reported the $FWHM_{(G)}$ versus I_D/I_G for all the samples at each gas. According to [8], this graphic show the evolution of the "crystallite size and defect" of the carbon. The most well crystalline sp^2 carbon is natural graphite, and it plotted closed to the origin of this graph (orange circle). The less organised carbon could be show ideally in the top of this diagram (Fig. 8) with $FWHM_{(G)}$ upper to ≈70 cm^{-1}. Fig. 8 a shows the results for the carbon obtain to a 100 % CO gas. All the data are very closed to the bottom part of the diagram with a moderate $FWHM_{(G)}$, due to the temperature of the experiment. As mentioned above, this result is in accordance with the lack of D band on the Raman spectra, due to the morphology of carbon in onion. The addition of 5 % of hydrogen in the gas mixture induce a moved to the right part of the diagram (Fig. 8 b), with an important increase of the $FWHM_{(G)}$. The increase of the H_2 content favoured an increase of the I_D/I_G ration and a relative staggering of the point (Fig. 8 c). This spreading should be moderated by the low quality of Raman spectra obtained for this test. The experiment using an analog of industrial gas (Fig. 8 d) with a CO/H_2 ratio closed to the gas mixture C, shows results similar to the data obtains in Fig. 8 c.

4.2.2 Microscopic characterisation of samples

To better understand the effect of sulphur on the inhibition of the carbon produced by the reverse Boudouard reaction catalysed by Fe_2O_3, the samples were observed after TGA experiments, by Scanning Electron Microscopy (SEM) and High-Resolution Transmission Electron Microscopy (HRTEM).

TEM micrographs of the samples, not exposed to SO_2, show the presence of small black iron carbide particles with a reduced size compared to the initial iron oxide grain size (Fig. 9). A part of the carbon forms nanofibres growing from Fe_3C particles. These carbon fibres are composed of poly-aromatic layers surrounding an amorphous core (Fig. 9 c–d).

The rounded shape of these particles may suggest a molten state. This observation was previously observed between 800–1000 °C [9, 10], and explained by Krause and Pötschke [1]: In the binary phase diagram Fe–C, the eutectic melting point drop from 1153 °C to temperature lower than 500 °C, and at this temperature droplets of carbon bearing iron are visible.

The sample exposed to 1000 ppm of $SO_{2(g)}$ exhibits a quite different morphology. EDS analysis reveals only the presence of iron carbide particles such as Fe_3C and/or Fe_5C_2 according to XRD. Considering their sizes, those particles do not seem to have been fragmented or fragmented to a lesser extent. A TEM micrograph for a sample exposed to 1000 ppm of $SO_{2(g)}$ is presented in Fig. 10 a. No filamentous carbon is observed on the micrograph and the iron carbide particles are systematically covered by a nanometer-sized thick shell. High resolution STEM-HAADF images show a two-layered shell (Fig. 10 b–c) The inner layer is very thin (0,5–1 nm). This inner layer is rich in sulphur with a rather high content of iron, which suggests the formation of an FeS iron sulphide.

5 Discussion about the mechanisms of carbon formation and carbon inhibition by sulphur

Under 100 % CO atmosphere, the carbon formation by the Boudouard reaction is a well know process. The iron oxides are reduced by CO and converted to iron carbide (cementite). Liquid iron/Fe_3C nanometric droplets are formed which dissolve carbon until the saturation limit. Carbon is segregated on the liquid surface droplet [1]. The catalytic deposit of carbon originates from a dissolution-precipitation mechanism of carbon.

The carbon has a high structural organisation and forms polyaromatic shells around big catalytic oxide particles.

When hydrogen is present, the reactions become more efficient. The phase transformations ($Fe_2O_3 \rightarrow FeO \rightarrow Fe \rightarrow Fe_3C$) result in a dramatic increase in the specific surface areas of catalytic particles. H_2 favours the nucleation and growth of carbon fibres on the iron-carbide particles.

Fig. 11 reports the different steps of the formation of carbon nanofibers by the reverse Boudouard reaction in CO–H_2 atmosphere:

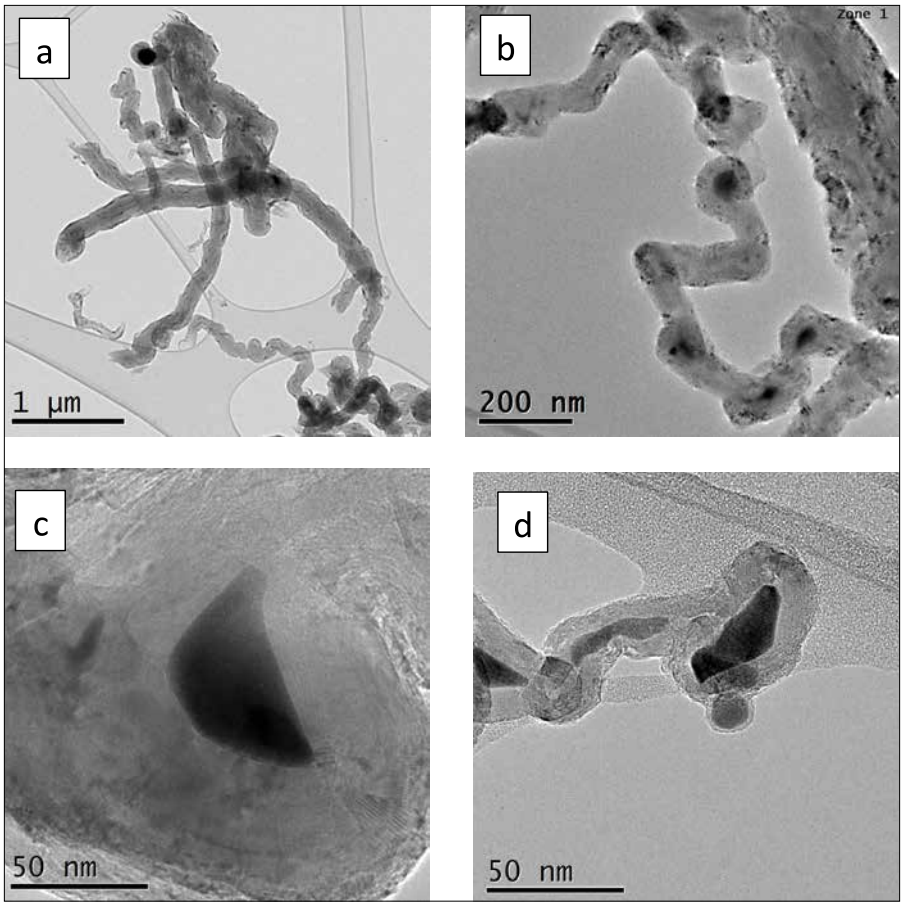

Fig. 9 a–d TEM micrograph of nano-carbon filaments for different catalysts formed at 600 °C in: a) 71 % CO, 3 % CO_2, 11 % H_2 and 15 % N_2 a Fe_2O_3 35 nm; b) Fe_2O_3 1–2 mm; c) Fe_3O_4 <5 µm; and d) FeO 2–5 µm

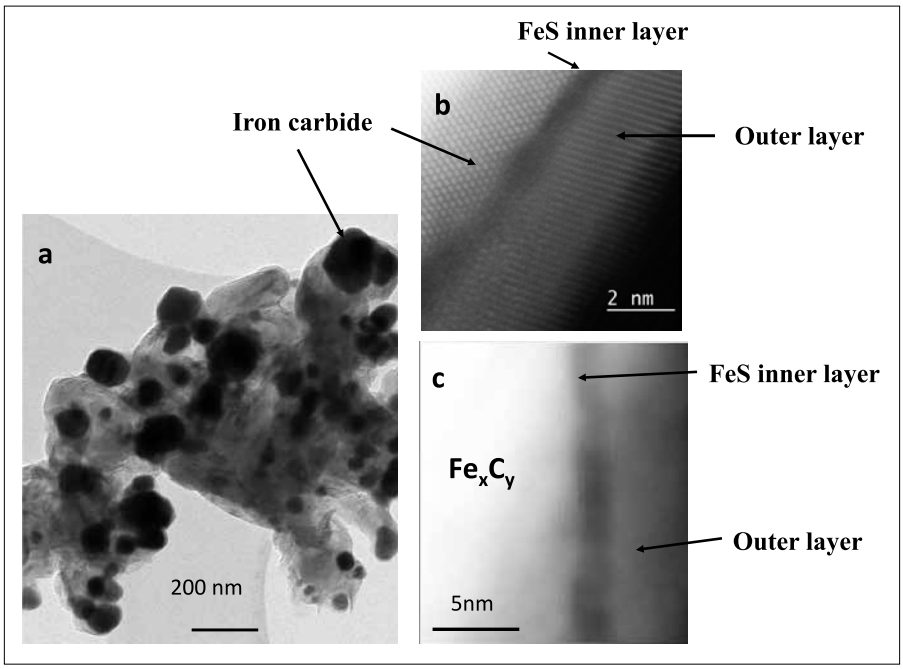

Fig. 10 a–c Micrographs of the sample after TGA experiments exposed to 1000 ppm of $SO_{2(g)}$: a) TEM image representative of the sample; b), c) high resolution HAADF-STEM images of a particle surrounded by a two-layer shell

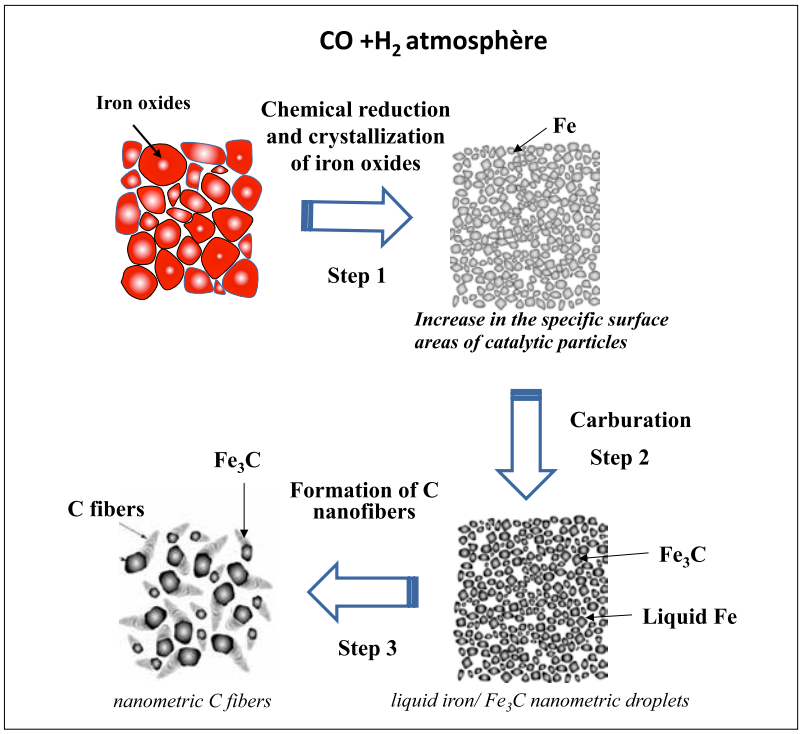

Fig. 11 Mechanism of carbon nanofibres formation by the reverse Boudouard reaction in CO–H_2 atmosphere

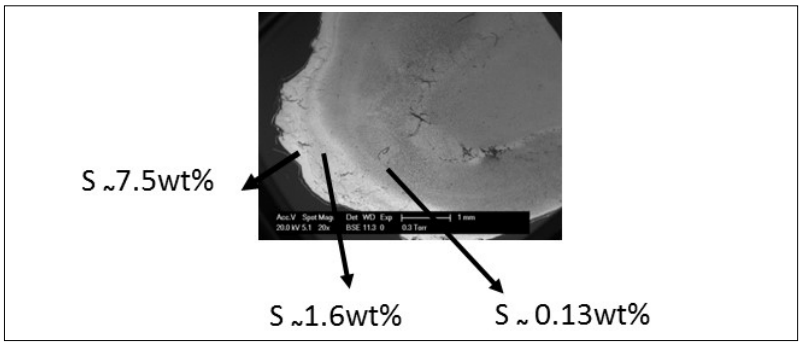

Fig. 12 SEM micrograph of iron sulphides at the surface of catalytic iron particles

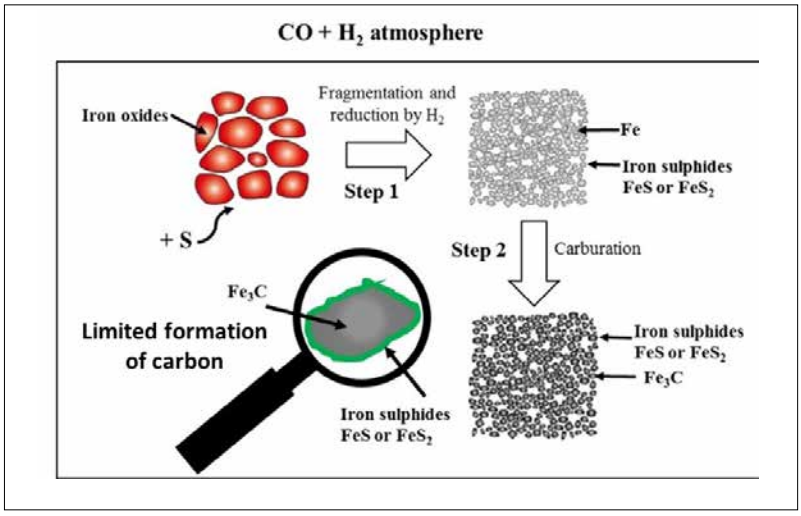

Fig. 13 Inhibition of carbon formation by S in CO–H_2 atmosphere

- Step 1: reduction by H_2 and CO with formation of suboxides of iron ($Fe_2O_3 \rightarrow FeO \rightarrow Fe$) recrystallization of particles and decrease of iron oxide size to nanometer-sized particles;
- Step 2: liquid iron/ Fe_3C nanometric droplets;
- Step 3: grow of polyaromatic carbon nanofibres.

The mechanism of the carbon formation is inhibited by sulphur or sulphates additions. This result is confirmed by 20 h experiments in laboratory. On the surface of the iron oxide particles, FeS or FeS_2 iron sulphides are formed (Fig. 12). The formation of these sulphides can be partial or total depending on the size of the iron oxide particles, the heating time and the reaction time.

Sulphur does not prevent the reduction of Fe_2O_3 by H_2 and CO and the fragmentation of the Fe_2O_3 grains. Nevertheless, it limits the formation of sp^2 carbon. Sulphur diffuse into the crystallite structure or through the grain boundaries. Moreover, it is not necessary to transform all the iron into iron sulphides to inhibit the carbon deposition by the reverse Boudouard reaction.

However, the FeS layer is not stable, S adsorption is a dynamic phenomenon and there are always some defects in the FeS layer which will lead to a slow continued carbon formation.

Fig. 13 reports the mechanism of carbon inhibition in CO–H_2 atmosphere.

6 Implication for industrial processes

The carbon formation from the Boudouard reaction and the nanocarbon formation were extensively studied for the last two decades. Nowadays, this phenomenon appears to be highly important for the development of new high temperature industrial processes. For example, in new energy field, the biomass and the waste gasification or the low C blast furnaces are highly vulnerable when the Boudouard reaction occurs. The refractory lining of these reactors could be highly damaged. Moreover, CO/H_2 gas will be efficiently used for reducing the power cost of industrial processes, and a technical solution should be developed for preserved refractory materials. Indeed, all these new developments are in relation with the global objective of reducing greenhouse gas emissions. The injection of H_2 gas

in CO mixture in refractory devices developed new challenges with the limitation of the damage of ceramics material. This destruction was well controlled in the case of only CO by empirical knowledge of refractories companies, however H_2 favoured the Boudouard reaction and eventually the formation of a specific sp^2 carbon as demonstrated in the paper. The problem is induced by the formation of carbon nanofibres in an abundant manner linked to the presence of CO + H_2 in the future industrial atmosphere. Consequently, this study is helpful for the development of laboratory and industrial solutions, for example by modification of carbon morphology.

The benefit effect of S to inhibit the formation of carbon was applied to develop CO/H_2 resistant refractories. Laboratory experiments were made using a commercial castable. The chemical composition [mass-%] of the castable is:

Al_2O_3	SiO_2	CaO	Fe_2O_3
81	16	2,5	0,6

To promote the formation of carbon and to increase the degradation of refractories, 5 mass-% Fe_2O_3 nanoparticles were mixed. Three different formula were prepared, and a low quantity of sulphur was incorporated in two samples:

- C1: castable + 5 mass-% Fe_2O_3;
- C2: castable + 5 mass-% Fe_2O_3 and 0,5 mass-% solid sulphur;
- C3: castable + 5 mass-% Fe_2O_3 and 3,3 mass-% $BaSO_4$.

After curing, the three castables were prefired in air at 900 °C, for 8 h. Then, they were submitted, for 5 h, at 600 °C under CO + H_2 reducing atmosphere (composition R). Reference powders of pure iron oxide were also tested under the same experimental conditions.

The castable C1 (with 5 mass-% Fe_2O_3) was destroyed by a "bursting reaction". A significant carbon deposit in the cementitious matrix was observed and analysed by Raman spectroscopy. The castables C2 and C3 containing S and $BaSO_4$ additives did not exhibit significant carbon deposit and were not damaged by the reverse Boudouard reaction (Fig. 14). These results were confirmed by Thermogravimetric Analyses (TGA), under reducing atmosphere: composition R: 71 % CO, 3 % CO_2, 11 % H_2, 15 % N_2.

However, the effect of S additives to inhibit the formation of carbon has limits: the sulphur additives become ineffective beyond 900 °C. In some industrial applications, the refractories are subjected to cyclic conditions: oxidising and reducing. Under these conditions, the stability of FeS and FeS_2 is not guaranteed.

An addition of sulphurous gas (100 ppm) in CO/H_2 gas should be an effective solution to limit the carbon formation and the damage of refractories.

7 Conclusion

The carbon deposit in refractories is catalysed by iron and iron oxides. This reaction is highly favoured by the presence of H_2. The mechanism of the catalytic decomposition of carbon monoxide via the Boudouard in the presence of H_2 is better understood. Two different carbons are formed in specific gas composition. In 100 % CO, the sp^2 carbon has a high structural organisation with important coherent domain diameter and formed polyaromatic shells around relatively big catalytic particles.

The addition of H_2 in CO favours the formation of polyaromatic carbon with nanofibre morphology. This morphology of carbon could be the cause of the destruction of refractory materials test in CO + H_2 atmosphere. Laboratory experimentations showed that sulphur additives inhibited the CO dissociation and the formation of carbon. The practical conclusions of this study will be applied to develop new CO/H_2 resistant refractories.

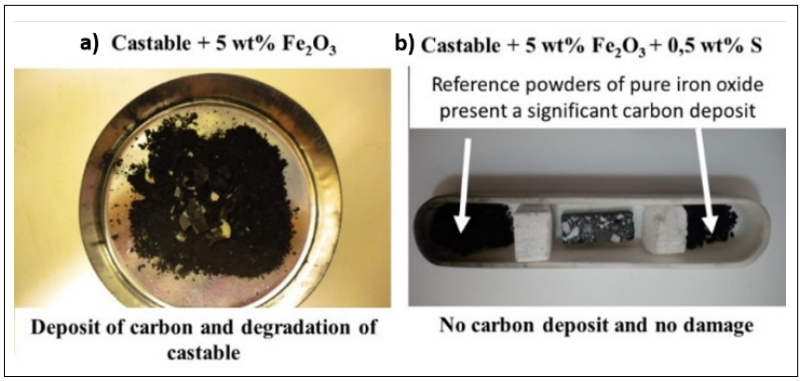

Fig. 14 Carbon deposit and destruction of C1 (a); effect of sulphur on C2 and C3 castables after exposure to reducing gas (b)

References

[1] Krause, O.; Pötschke, J.: The predictability of CO resistance of refractory materials by state-of-the-art test methods – a technical and scientific approach. Interceram **57** (2008) 176–180

[2] Bost, N.; et al.: The catalytic effect of iron oxides on the formation of nanocarbon by the Boudouard reaction. J. Europ. Ceram. Soc. **36** (2016) 2133–2142

[3] Walker, P.L.; Raicszawski, J.F.; Imperial, G.R.: Carbon formation from carbon monoxide-hydrogen mixtures over iron catalysts. J. Phys. Chem. **63** (1959) 140–149

[4] Turkdogan, E.T.; Vinters, J.V.: Catalytic effect of iron on decomposition of carbon monoxide: I. carbon deposition in H_2–CO mixtures. Metall. Trans. **5** (1974) 11–19

[5] Berry, T.F.; Ames, R.N.; Snow, R.B.: Influence of impurities and role of iron carbides in deposition of carbon from carbon monoxide. J. Amer. Ceram. Soc. **39** (1956) 308–318

[6] Bost, N.; et al.: Probing the structural organization of sp^2 carbons obtained by the Boudouard reaction using in situ Raman scattering in reducing conditions. Vibrational Spectroscopy **87** (2016) 157–163

[7] Ammar, M.R.; Rouzaud, J.N.: How to obtain a reliable structural characterization of polished graphitized carbons by Raman microspectroscopy. J. Raman Spectroscopy **43** (2011) 207–221

[8] Ammar, M.R.; et al.: Characterizing various types of defects in nuclear graphite using Raman scattering: heat treatment, ion irradiation and polishing. Carbon **95** (2015) 364–373

[9] Yazdanbakhsh, A.; et al.: Challenges and benefits of utilizing carbon nanofilaments in cementitious materials. J. of Nanomaterials 2012 (2012) 2012, Article ID 371927, 1–8

[10] Drzal, L.; Fukushima, H.: Conference proceedings of high performance fillers, paper 15, 2006